Available online at www.sciencedirect.com

SciVerse ScienceDirect

Scripta Materialia 68 (2013) 118–121

Scripta MATERIALIA

www.elsevier.com/locate/scriptamat

Grain-boundary strengthening in nanocrystalline chromium and the Hall–Petch coefficient of body-centered cubic metals

D. Wu,[a] Junyan Zhang,[b] J.C. Huang,[c] H. Bei[d] and T.G. Nieh[a,*]

[a]*Department of Materials Science and Engineering, University of Tennessee, Knoxville, TN 37996, USA*
[b]*State Key Laboratory of Solid Lubrication, Lanzhou Institute of Chemical Physics, Chinese Academy of Sciences, Lanzhou 730000, China*
[c]*Department of Materials and Optoelectronic Science, National Sun Yat-Sen University, Kaohsiung 804, Taiwan, ROC*
[d]*Materials Science and Technology Division, Oak Ridge National Laboratory, Oak Ridge, TN 37831, USA*

Received 23 August 2012; revised 23 September 2012; accepted 26 September 2012
Available online 2 October 2012

Nanocrystalline Cr (nc-Cr) was synthesized by electrodeposition. Samples with various grain sizes (19–57 nm) were prepared by annealing the as-deposited sample. Microstructures were examined using X-ray and electron microscopy, and the mechanical properties were evaluated using nanoindentation. The strength of nc-Cr samples apparently obeyed the classical Hall–Petch relationship. It was found that hardening potency caused by grain refinement was generally higher in body-centered cubic metals than that in face-centered cubic and hexagonal close-packed metals. A possible explanation was offered.

Keywords: Grain boundaries; Nanocrystalline metal; Nanoindentation; Hall–Petch effect

It is a conventional knowledge that grain refinement can increase the strength of a polycrystalline metal. In fact, the classical Hall–Petch (H-P) relationship [1,2] correlating strength with grain size has been widely applied over many decades. Recently, an inverse H-P relationship was observed in some metals and alloys with nanoscale grain sizes, e.g. Ni [3], Cu [4] and Ni–W [5]. Whereas many of these studies were conducted on nanocrystalline (nc) face-centered cubic (fcc) [6–9] and hexagonal close-packed (hcp) metals [10], a limited number of studies have been reported in body-centered cubic (bcc) metals [11,12]. This is probably due to the fact that nc-metals and alloys are mainly produced by electrodeposition and the reduction potentials for bcc transition metals (e.g. Mo, W, Ta and Nb), except Cr, are relatively high. The electrolyte for electrodeposition is generally water based, and water would be electrolyzed to hydrogen and oxygen before the metal ions were reduced to their metallic states.

In the present study, the effect of grain size on the hardness (or strength) of nc-Cr samples was initially evaluated by a nanoindentation technique, then a comprehensive survey and systematic discussion on the hardening potency of grain size in metals with different crystalline structures (i.e. bcc, fcc and hcp) was carried out.

The nc-Cr coatings were electrodeposited on a stainless steel substrate in a modified "Sargent" bath, containing CrO_3– (250 g l^{-1}), H_2SO_4 (2.5 g l^{-1}) and a small amount of "Ca-2000" additives (Xinhua Yatai Chemical Tech Ltd, China), with a current density 40 A dm^{-2} at 55 °C, as reported previously [13]. Platinum wire was used as a counter electrode. The as-deposited film had a thickness of about 100 μm and an average grain size of about 19 nm. Larger grain sizes were obtained by annealing the as-deposited film at different temperatures (350, 400, 450, 550 and 600 °C) for 1 h in air. Samples annealed at X °C are denoted as CrX herein (for example, Cr600 is the sample annealed at 600 °C). The surface of the annealed samples was polished to remove any possible oxide before the nanoindentation tests were carried out. A coarse-grained bulk Cr sample was also prepared using the arc-melting method for comparison. All Cr samples were examined for grain size and purity by X-ray diffraction (XRD) using Cu K_α radiation at 45 kV and 40 mA. The grain sizes of the nc-Cr samples were also measured from TEM micrographs.

For the nanoindentation tests, all the specimens were initially mounted in epoxy resin and then ground and

* Corresponding author. Tel.: +1 865 974 5328; e-mail: tnieh@utk.edu

1359-6462/$ - see front matter © 2012 Acta Materialia Inc. Published by Elsevier Ltd. All rights reserved.
http://dx.doi.org/10.1016/j.scriptamat.2012.09.025

polished to a mirror finish. Tests were carried out on a Triboindenter (Hysitron, Minneapolis, MN) with a Berkovich indenter at room temperature. At least 10 indents with a fixed displacement were conducted on each sample, the indent depth was 160 nm and the loading rate ranged from 0.9 to 1.4 mN s^{-1}. The indenter was calibrated both before and after nanoindentation.

The XRD pattern from the as-deposited Cr indicates a bcc structure, as shown in Figure 1. Truncated patterns near the (1 1 0) diffraction peak from samples annealed at different temperatures are included in the inset. The grain sizes of these nc-Cr samples were estimated from the (1 1 0) diffraction peaks using the Debye–Scherrer formula and the results are summarized in Table 1; the grain sizes ranged from 19 to 57 nm.

Since XRD usually yields a smaller grain size [14], direct measurement was also carried out using TEM. TEM micrographs of the planar view (Fig. 2(a) and (c)) and cross-sectional view (Fig. 2(b) and (d)) of the

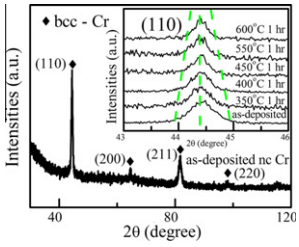

Figure 1. XRD pattern of the as-deposited nc-Cr coating and the XRD patterns around the diffraction peak (1 1 0) for the as-deposited and annealed nc-Cr specimens (inset).

Table 1. Grain size and hardness of nc-Cr samples.

Specimen	Grain size (XRD) (nm)	Grain size (TEM) (nm)	Hardness (GPa)
As-deposited Cr	19	24	12.22 ± 0.06
Cr350	22	–	11.71 ± 0.07
Cr400	26	–	10.55 ± 0.07
Cr450	33	–	10.09 ± 0.05
Cr550	41	–	9.31 ± 0.08
Cr600	57	82	7.98 ± 0.07

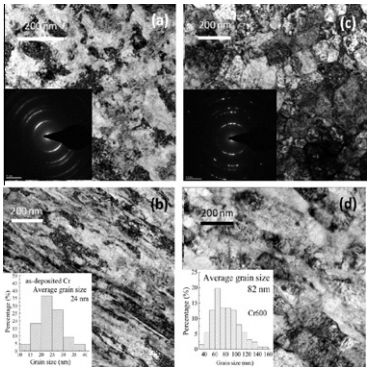

Figure 2. TEM micrographs taken from nc-Cr coatings: planar view and SAED pattern (insets) for (a) as-deposited Cr and (c) Cr600. Cross-sectional view and grain size distribution (insets) for (b) as-deposited Cr and (d) Cr600.

as-deposited Cr and Cr600 indicate a columnar grain along the growth direction of electrodeposition. The non-uniform diffraction rings shown in the selected diffraction patterns suggest a strong (2 1 1) texture that is often observed in electrodeposits [5]. It appears that the majority of grain boundaries are high angled.

The TEM micrographs also reveal that the grain size of the as-deposited Cr film is about 24 nm, which increases to about 82 nm subsequent to annealing at 600 °C. As expected, these values are larger than those estimated by XRD, but both data sets appear to scale with each other (Fig. 3). It is noted that no oxide/carbide precipitate was observed in the TEM microstructure, suggesting impurity atoms were dispersed in the Cr lattice as solutes. These impurities can affect the resultant hardness value. However, in the current study of the grain size effect, all specimens initially came from the same batch; consequently, the impurity content in each test sample was the same. If there is any solid solution or particle strengthening caused by these impurities, their contributions to the hardness of the test samples would, in practice, be similar.

Hardness values of the nc-Cr samples with various grain sizes were measured and the results are presented in Figure 3; the error bar for each hardness value is less than 1%. It is evident that, within the current grain size range, the hardness values follow the classical Hall–Petch relationship,

$$H = H_0 + k_{HP} d^{-1/2} \quad (1)$$

where H_0 is the intrinsic hardness of Cr, which can, in principle, be estimated from the coarse-grained Cr (grain size = 0.5 mm), d is average grain size and k_{HP} is the Hall–Petch coefficient. There is no apparent indication of a Hall–Petch inversion, such as that observed in fcc nc-Ni or Ni–W [3,5,15].

To make a direct comparison of the strength–grain size relationship, data obtained from several ultrafine/nanocrystalline metals, including Mo and Fe, Ni and Cu, and Mg, Zn and Ti, are also presented in a Hall–Petch plot, as shown in Figure 4(a). Despite some data variations, it is apparent that the slope, i.e. the Hall–Petch coefficient, k_{HP}, for bcc metals (black symbols) is generally much higher than that for fcc (blue symbols) and hcp (red symbols) metals. This is consistent with the previous conclusion [14] that grain boundaries in bcc metals seems to be more efficient in blocking dislocation motion than that in the fcc/hcp metals.

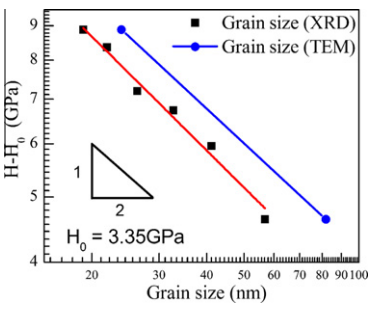

Figure 3. Reduced hardness as a function of grain size, indicating that nc-Cr follows the Hall–Petch relationship closely.

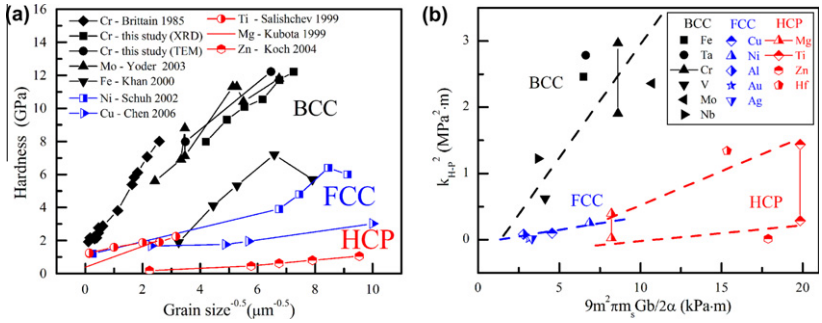

Figure 4. (a) Comparison of Hall–Petch relationship and (b) the square of the Hall–Petch coefficient k_{HP}^2as a function of $9m^2\pi m_s Gb/2\alpha$ for ultrafine and nanopolycrystalline metals with different crystalline structures: bcc (black symbol), fcc (blue) and hcp (red). (For interpretation of the references to color in this figure legend, the reader is referred to the web version of this article.)

According a dislocation pile-up model [2], Armstrong [16] suggested the incipient plastic deformation as a process of dislocation source operation by the stress concentration at the grain boundary. Following the relationship between the stress concentration and the critical shear stress for source operation [17], the Hall–Petch coefficient k_{HP} can be expressed as

$$k_{HP} = 3m(\pi m_s \tau_c Gb/2\alpha)^{1/2} \quad (2)$$

where m is the Taylor factor relating tensile strength to the resolved shear stress of a polycrystal, m_s is the Sachs orientation factor, G is the shear modulus, b is the dislocation Burgers vector, an average dislocation character is expressed in the factor $\alpha = 2(1-\nu)/(2-\nu)$, with ν being Poisson's ratio, τ_c is the resolved shear stress required to operate the dislocation source near the grain boundary, and the ratio 3 is from the well-accepted Tabor's relation between indentation hardness and yield strength of a material. As indicated in Eq. (2), k_{HP} is a function of the shear modulus, Burgers vector, Poisson's ratio and, in particular, the critical shear stress for dislocation nucleation from grain boundaries.

The Hall–Petch coefficient k_{HP} for a number of polycrystalline metals with bcc, fcc and hcp structures are summarized in Table 2. To obtain τ_c from Eq. (2), the square of k_{HP} is plotted as a function of the parameter $9m^2\pi m_s Gb/2\alpha$ for these metals in Figure 4(b). The slope of the curve is τ_c, the resolved shear stress necessary to propagate plastic flow across the grain boundary. The data in Figure 4(b) can be separated into two groups: one for bcc and the other for the close-packed fcc and hcp metals. Also, the slope for bcc metals is notably higher than that for fcc and hcp metals, clearly suggesting a larger critical shear stress for the propagation of plastic deformation cross-grain boundaries in bcc metals. Specifically from Figure 4(b), the τ_c for bcc metals is evaluated to be 350 MPa, which is about 6 times for fcc (56 MPa) and 4 times for the upper-bound value for hcp (90 MPa) metals.

Armstrong and Rodriguez [44] also suggested that τ_c was related to the stage-III shear stress τ_{III} for single-crystal metals. A summary of τ_c and τ_{III} for bcc, fcc and hcp metals is listed in Table 3. It is evident that both τ_c and τ_{III} for bcc metals are significant larger than those for the fcc metals. This was expected, since it has been demonstrated that the activation energy for the nucleation of partial dislocations is energetically favored in fcc and hcp metals [45], in contrast to bcc metals, where nucleation of full dislocations is favored [46]. It is also noted that τ_c is generally larger than τ_{III}. The discrepancy is probably associated with the grain-boundary structure and chemistry. Whereas τ_{III} is mainly determined by dislocation interactions within the interior of

Table 2. Comparison of Hall–Petch coefficient of ultrafine/nanocrystalline metals.

Metals	G (GPa)	b (nm)	k_{HP} (MPa·μm$^{0.5}$)	References
bcc Fe	82	0.248	1589	[18]
bcc Ta	69	0.286	1669	[19]
bcc Cr	115	0.250	2561	[20]
			1723	[21]
			1380	This study
bcc V	46.4	0.262	789	[22]
bcc Mo	120	0.273	1536	[23]
bcc Nb	37.5	0.285	1051	[24]
fcc Cu	48	0.255	316	[25]
fcc Ni	76	0.249	502	[26]
fcc Al	26	0.286	285	[27]
fcc Au	27	0.289	60–180	[28]
fcc Ag	30	0.289	133	[29]
hcp Mg	17	0.466	630	[30]
			69–237	[31]
hcp Zn	43	0.414	120	[32]
hcp Ti	44	0.424	322–750	[33]
			1200	[34]
hcp Hf	30	0.459	1157	[35]

Table 3. Comparison of τ_c according to Armstrong's model and stage III shear stress, τ_{III}, for bcc, fcc and hcp single crystals.

Metals	k_{HP} (MPa μm$^{0.5}$)	τ_c (MPa)	τ_{III} (MPa)	References for τ_{III}
bcc Cr	1380	221	141	[36]
bcc Ta	1669	420	220	[37]
bcc Fe	342–1568.5	18–379.1	20–50	[38,39]
bcc Mo	1536	221	180	[40]
fcc Cu	316	21.9	22.2	[41]
fcc Ni	502	36.7	27.8	[41]
fcc Al	285	29	4.6	[41]
fcc Au	60–180	1.1–10.3	8.1	[41]
fcc Ag	133–384	5.3–44.3	18.62	[41]
hcp Mg	153[a]	2.85	2	[42]
hcp Zn	120	0.8	0.55–0.7	[43]

[a] The k_{HP} value for slip-dominated deformation is used for the calculation.

grains, τ_c is controlled by the nature of the grain boundaries. It has been demonstrated before that impurity segregation at grain boundaries can significantly affect the k_{HP} value in bcc Fe [47,48] and fcc Ni [49]. However, it should also be noted that, within each structure group (i.e. fcc or bcc), τ_c and τ_{III} agree reasonably well, at least within a similar magnitude.

In this study, we demonstrate that nanocrystalline Cr obeys the Hall–Petch relationship at grain sizes as small as 19 nm. We also find that the hardening potency by grain refinement is more effective in bcc metals than in fcc and hcp metals, and specifically the Hall–Petch coefficient, k_{HP}, is around 1500 MPa·μm$^{0.5}$ for many bcc metals but no more than 600 MPa·μm$^{0.5}$ for fcc metals. This higher k_{HP} in bcc metals results from the higher resolved shear stress necessary to propagate plastic flow across the grain boundary, which, in turn, is caused by the higher activation energy required for the nucleation of full dislocations in bcc as compared to the partial dislocations in fcc metals. The nature of grain boundaries – in particular, the chemistry – may also contribute to the high k_{HP} since bcc metals are susceptible to impurity segregation.

This work was supported by the National Science Foundation under Contract DMR-0905979 (T.G.N. and D.W.). H.B. was supported by the US Department of Energy, Basic Energy Sciences, Materials Sciences and Engineering Division. We would like to thank Dr. Ian Liu, NSYSU, for his technical contribution of the TEM work.

[1] N.J. Petch, J. Iron Steel Inst. 174 (1953) 25–28.
[2] E.O. Hall, Proc. Phys. Soc. Lond. B 64 (1951) 747–753.
[3] C.A. Schuh, T.G. Nieh, T. Yamasaki, Scripta Mater. 46 (2002) 735–740.
[4] S.Y. Chang, T.K. Chang, J. Appl. Phys. 101 (2007) 033507.
[5] C.A. Schuh, T.G. Nieh, H. Iwasaki, Acta Mater. 51 (2003) 431–443.
[6] F. Dalla Torre, H. Van Swygenhoven, M. Victoria, Acta Mater. 50 (2002) 3957–3970.
[7] N. Hansen, Scripta Mater. 51 (2004) 801–806.
[8] H. Conrad, K. Jung, Mater. Sci. Eng. A: Struct. Mater. 391 (2005) 272–284.
[9] D. Wolf, V. Yamakov, S.R. Phillpot, A. Mukherjee, H. Gleiter, Acta Mater. 53 (2005) 1–40.
[10] K. Saber, C.C. Koch, P.S. Fedkiw, Mater. Sci. Eng. A 341 (2003) 174–181.
[11] D. Jang, M. Atzmon, J. Appl. Phys. 93 (2003) 9282–9286.
[12] D. Jia, K.T. Ramesh, E. Ma, Acta Mater. 51 (2003) 3495–3509.
[13] Z.X. Zeng, J.Y. Zhang, J. Phys. D: Appl. Phys. 41 (2008).
[14] M. Zhang, B. Yang, J. Chu, T.G. Nieh, Scripta Mater. 54 (2006) 1227–1230.
[15] T. Yamasaki, Scripta Mater. 44 (2001) 1497–1502.
[16] R.W. Armstrong, Acta Metall. 16 (1968) 347–355.
[17] R. Armstrong, R.M. Douthwaite, I. Codd, N.J. Petch, Philos. Mag. 7 (1962) 45–58.
[18] A.S. Khan, H.Y. Zhang, L. Takacs, Int. J. Plast. 16 (2000) 1459–1476.
[19] A.F. Jankowski, J. Go, J.P. Hayes, Surf. Coat. Technol. 202 (2007) 957–961.
[20] C.P. Brittain, R.W. Armstrong, G.C. Smith, Scripta Metall. 19 (1985) 89–91.
[21] V. Provenzano, R. Valiev, D.G. Rickerby, G. Valdre, Nanostruct. Mater. 12 (1999) 1103–1108.
[22] A.F. Jankowski, J.P. Hayes, C.K. Saw, Philos. Mag. 87 (2007) 2323–2334.
[23] K.B. Yoder, A.A. Elmustafa, J.C. Lin, R.A. Hoffman, D.S. Stone, J. Phys. D: Appl. Phys. 36 (2003) 884–895.
[24] A.M. Omar, A.R. Entwisle, Mater. Sci. Eng. 5 (1970) 263–270.
[25] J. Chen, L. Lu, K. Lu, Scripta Mater. 54 (2006) 1913–1918.
[26] G.D. Hughes, S.D. Smith, C.S. Pande, H.R. Johnson, R.W. Armstrong, Scripta Metall. 20 (1986) 93–97.
[27] A.S. Khan, B. Farrokh, L. Takacs, Mater. Sci. Eng. A: Struct. Mater. 489 (2008) 77–84.
[28] Y.H. Chew, C.C. Wong, F. Wulff, F.C. Lim, H.M. Goh, Thin Solid Films 516 (2008) 5376–5380.
[29] X.Y. Qin, X.J. Wu, L.D. Zhang, Nanostruct. Mater. 5 (1995) 101–110.
[30] K. Kubota, M. Mabuchi, K. Higashi, J. Mater. Sci. 34 (1999) 2255–2262.
[31] M.R. Barnett, Z. Keshavarz, A.G. Beer, D. Atwell, Acta Mater. 52 (2004) 5093–5103.
[32] X. Zhang, H. Wang, R.O. Scattergood, J. Narayan, C.C. Koch, Mater. Sci. Eng. A: Struct. Mater. 344 (2003) 175–181.
[33] C.Y. Hyun, J.H. Lee, H.K. Kim, Res. Chem. Intermed. 36 (2010) 629–638.
[34] R.J. Lederich, S.M.L. Sastry, J.E. O'Neal, B.B. Rath, Mater. Sci. Eng. 33 (1978) 183–188.
[35] E. Cerreta, C.A. Yablinsky, G.T. Gray III, S.C. Vogel, D.W. Brown, Mater. Sci. Eng. A: Struct. Mater. 456 (2007) 243–251.
[36] C.N. Reid, A. Gilbert, G.T. Hahn, Trans. TMS-AIME 239 (1967) 467–473.
[37] R. Kapoor, S. Nemat-Nasser, Scripta Mater. 40 (1998) 159–164.
[38] V. Novak, S. Kadeckova, B. Sestak, N. Zarubova, Cryst. Res. Technol. 19 (1984) 781–791.
[39] D. Brunner, J. Diehl, Phys. Status Solidi A 124 (1991) 155–170.
[40] L. Hollang, D. Brunner, A. Seeger, Mater. Sci. Eng. A: Struct. Mater. 319–321 (2001) 233–236.
[41] J.F. Bell, Philos. Mag. 11 (1965) 1135–1156.
[42] B. Bhattacharya, M. Niewczas, Philos. Mag. 91 (2011) 2227–2247.
[43] D.H. Lassila, M.M. LeBlanc, J.N. Florando, Metall. Mater. Trans. A 38 (2007) 2024–2032.
[44] R.W. Armstrong, P. Rodriguez, Philos. Mag. 86 (2006) 5787–5796.
[45] H. Van Swygenhoven, P.M. Derlet, A. Hasnaoui, Phys. Rev. B 66 (2002) 024101.
[46] L. Wang, H. Bei, T.L. Li, Y.F. Gao, E.P. George, T.G. Nieh, Scripta Mater. 65 (2011) 179–182.
[47] K. Takeda, N. Nakada, T. Tsuchiyama, S. Takaki, ISIJ Int. 48 (2008) 1122–1125.
[48] J. Takahashi, K. Kawakami, K. Ushioda, S. Takaki, N. Nakata, T. Tsuchiyama, Scripta Mater. 66 (2012) 207–210.
[49] X.F. Zhang, T. Fujita, D. Pan, J.S. Yu, T. Sakurai, M.W. Chen, Mater. Sci. Eng. A: Struct. Mater. 527 (2010) 2297–2304.